

The Open Polymers 2026 (OPoly26) Dataset and Evaluations

Daniel S. Levine^{1,*†}, Nicholas Liesen^{2,*}, Lauren Chua³, James Diffenderfer², Helgi Ingolfsson², Matthew P. Kroonblawd², Nitesh Kumar³, Amitesh Maiti², Supun S. Mohottalalage², Muhammed Shuaibi¹, Brian Van Essen², Brandon M. Wood¹, C. Lawrence Zitnick¹, Samuel M. Blau^{3,†}, Evan R. Antoniuk^{2,†}

¹FAIR at Meta, ²Lawrence Livermore National Laboratory, ³Lawrence Berkeley National Laboratory
^{*}Co-first Author, [†]Co-corresponding Author

Polymers—macromolecular systems composed of repeating chemical units—constitute the molecular foundation of living organisms, while their synthetic counterparts drive transformative advances across medicine, consumer products, and energy technologies. While machine learning (ML) models have been trained on millions of quantum chemical atomistic simulations for materials and/or small molecular structures to enable efficient, accurate, and transferable predictions of chemical properties, polymers have largely not been included in prior datasets due to the computational expense of high quality electronic structure calculations on representative polymeric structures. Here, we address this shortcoming with the creation of the Open Polymers 2026 (OPoly26) dataset, which contains more than 6.57 million density functional theory (DFT) calculations on up to 360 atom clusters derived from polymeric systems, comprising over 1.2 billion total atoms. OPoly26 captures the chemical diversity that makes polymers intrinsically tunable and versatile materials, encompassing variations in monomer composition, degree of polymerization, chain architectures, and solvation environments. We show that augmenting ML model training with the OPoly26 dataset improves model performance for polymer prediction tasks. We also publicly release the OPoly26 dataset to help further the development of ML models for polymers, and more broadly, strive towards universal atomistic models.

Dataset Updated with OPoly26: <https://huggingface.co/facebook/OMol25>

Code: <https://github.com/facebookresearch/fairchem>

Correspondence: D.S.L. (levineds@meta.com), S.M.B. (smblau@lbl.gov), E.R.A. (antoniuk1@lbl.gov)

1 Introduction

Polymers are ubiquitous in modern life, employed in diverse areas from common consumer packaging to cutting-edge technologies, such as additive manufacturing and lithium-ion batteries[1–3]. Simultaneously, the stability and tunability that makes polymers so useful has also placed them at the forefront of societal issues including the accumulation of plastic waste and the prevalence of microplastics[4, 5]. As a result, there is an urgent need to innovate in polymer design and synthesis, such that next-generation polymeric materials can be rapidly developed to meet these emerging societal and technological challenges.

Polymers are composed of long chains of repeating chemical units (monomers) whose architecture and composition can be systematically varied, thereby providing an additional dimension of tuning material properties. However, understanding structure-property relationships in polymers is inherently complex since it is dependent on capturing both atomic-scale interactions such as covalent bonds, hydrogen bonding, and dispersion, as well as interactions between collections of polymer chains, such as chain entanglements[6–8]. Despite these challenges, computational modeling has become an essential tool for understanding polymer chemistry, providing a detailed atomistic description of polymer structure and dynamics[9]. Predictive insight into polymer degradation processes could unlock new materials properties and recycling schemes, which are needed to address the ecological impact of polymer materials.

Polymer simulations leverage different computational methods depending on the length-scale and time-scale of interest. Density functional theory (DFT) calculations can provide a high-accuracy description of the electronic structure of monomers/oligomers of O(100) atoms[10, 11]. While DFT is employed to study the reactivity and

optoelectronic properties of small oligomers, it is too computationally burdensome to simulate larger systems or polymer chain dynamics. Molecular dynamics (MD) simulations with classical force fields (FFs) have long been used to simulate the dynamics of polymers with typical length-scales up to 100 Å and time-scales up to 100 ns[9, 12, 13]. A number of classical nonreactive FFs developed in the 1990s, including COMPASS, PCFF, OPLS and DREIDING, have been used for decades to perform MD simulations on polymer systems[14–18]. Typically, these FFs have been parameterized so as to reproduce a set of reference experimentally observed polymer properties, such as crystal structure parameters or densities.[14, 15] However, classical FFs cannot accurately describe reactivity and exhibit limited transferability to chemical environments and conditions that they were not explicitly trained on.[9]

Machine Learning Interatomic Potentials (MLIPs) have recently emerged as transformative tools for atomistic simulations.[19–21] When trained on large datasets of DFT calculations, MLIPs can provide near-DFT-level accuracy energy and force predictions with near-classical-FF speed.[22] MLIPs thus have the potential to enable large-scale polymer molecular dynamics simulations over long time scales while faithfully describing atomistic interactions and reactivity. Recently, large-scale pre-trained MLIPs have been developed that train on DFT calculations covering multiple material types, including molecules, metal-organic frameworks, and crystalline materials.[19] While these MLIPs seek to be chemically universal, they do not include polymeric simulations in their training data, primarily due to the lack of suitable open-source polymer DFT datasets. Nevertheless, ensuring that MLIPs accurately generalize to polymers is essential for building a true atomistic foundation model[23].

The dearth of polymer DFT datasets for MLIP training can be partially attributed to the large computational expense required to sufficiently sample the vast chemical and structural space of polymer chemistries. While the recently released Open Molecules 2025 (OMol25) dataset[24] did include large polypeptide structures, in addition to small molecules, electrolytes, and metal complexes, it did not sample polymer structures more broadly. Meanwhile, classical polymer force field models are traditionally parameterized on a single polymer composition or narrow polymer family, such as polycarbonates[14]. Similarly, specialized polymer MLIP models have been trained on O(1000) polymer structures originating from *ab initio* MD.[25] The recently published SimPoly effort reported a dataset for MLIP training consisting of DFT calculations on 680,000 polymer configurations[26]. While these configurations were sampled from just 130 unique polymer compositions and cover only stable homopolymers, SimPoly was a major advance over previous work, and the curated set of experimentally measured bulk polymer properties should become a standard evaluation for molecular MLIPs going forward.

Here, we present the Open Polymers 2026 (OPoly26) Dataset—a large-scale, openly available resource designed to enable the development of MLIPs for polymeric systems (Figure 1). Diverse polymeric structures are obtained by simulating polymer structure dynamics, including molecular dynamics (MD) simulations of 94k unique amorphous polymer simulation cells for a cumulative total of over 239,000 ns. We extract substructures from these larger polymeric systems, capping dangling bonds with hydrogens as necessary, and form the MLIP training data from over 6.57 million DFT single-point calculations including 1.2B total atoms. OPoly26 was specifically designed to capture the vast diversity of chemical environments found in polymer materials, spanning various linear chain architectures, molecular weight distributions, solvation environments, condensed-phase reactions, and polymer-ion interactions. OPoly26 also used the identical DFT settings as OMol25, making it trivial to combine the datasets for MLIP training. We demonstrate that an MLIP trained on a combination of OPoly26 and OMol25 is more accurate for polymer systems than an MLIP trained on OMol25 alone without regressing on the performance for other molecular chemistry domains. To encourage the open development of improved MLIP models, we provide all of the OPoly26 data with a CC-BY-4.0 license.

2 Open Polymers 2026 Dataset

In order to sample a broad range of polymer structures in OPoly26, we include diverse monomeric repeat units, backbone structures, and supramolecular arrangements. In Section 2.1, we describe the various sources of monomers which span the field of polymer science, including optical polymers, fluorinated polymers, polymer electrolytes, and more. Those monomers are assembled into a range of polymer architectures (Section 2.2), which were simulated with multiple techniques to generate diverse 3D structures for each polymer system

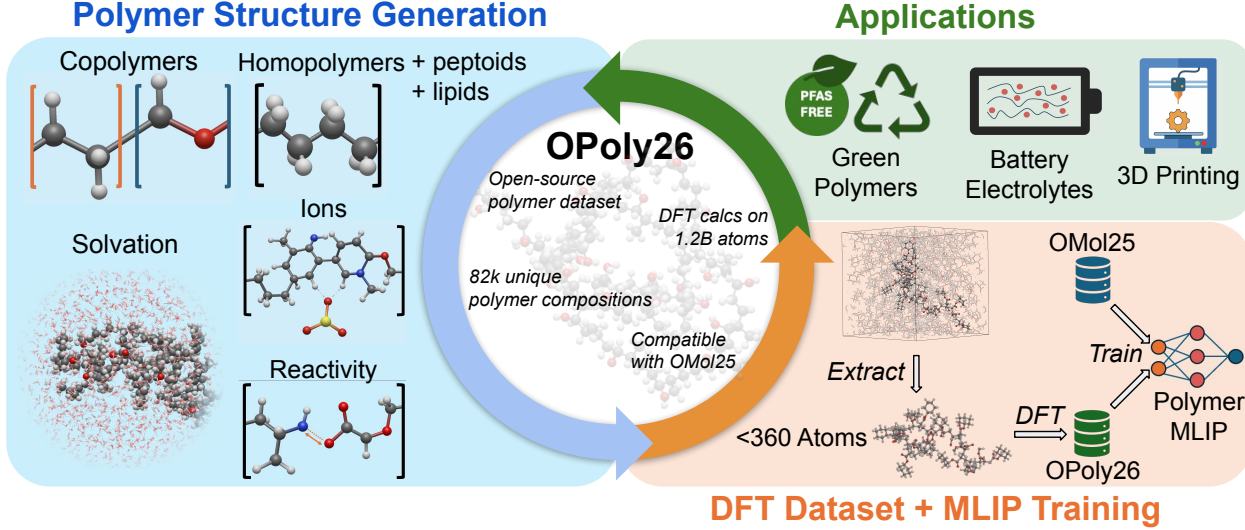


Figure 1 Overview of OPoly26. We generate diverse polymeric structures that cover a broad spectrum of polymer chemistries including homopolymers and highly diverse copolymers, as well as interactions between polymers and solvent molecules and ionic species. We then extract $>6M$ substructures with <360 atoms, capping dangling bonds with hydrogens as necessary, and simulate each with DFT. We train MLIP models on both the OPoly26 and OMol25 datasets, which employed identical DFT settings, to ensure model generalization across molecular chemistry domains, unlocking improved simulation capabilities in a range of high-impact applications.

(Section 2.3-2.4). Finally, we extract a total of 6.57 million unique substructures from these larger polymer systems and perform high-throughput DFT calculations to generate the OPoly26 dataset for MLIP training (Figure 2).

Altogether, the OPoly26 dataset is sourced from 2,444 unique monomers, with more than 1.2 billion total atoms across all the DFT calculations. The MD trajectories alone consist of 43,176 simulation cells of ~ 300 atoms and 51,260 simulation cells of ~ 5000 atoms, simulated over a cumulative 239,000 ns. These polymer systems include various linear chain architectures, solvation environments, chain lengths, and comonomer ratios, thereby capturing the structural complexities and diversity of atomistic interactions in polymers more comprehensively than prior homopolymer-only datasets. The OPoly26 dataset contains more than 6.57 million DFT calculations and required $\sim 1.2B$ CPU core-hours.

2.1 Polymer Compositions

Polymers are an extremely versatile class of materials that can include a diverse range of chemistries in their repeat units. In the following subsections, we outline the categories of polymer compositions in OPoly26 and how they were sampled. Our detailed procedure for obtaining all polymer compositions is available in Appendix B.

2.1.1 Traditional Polymers

For a representative set of commonly used synthetic polymers, we leveraged the collection of homopolymers from the RadonPy benchmark set [27]. Notably, these polymers have the largest number of experimental measurements in the PolyInfo database,[28] indicating that they are widely used and relevant materials. We further augmented this set with hand-picked polymer compositions from textbooks to broaden the distribution of represented polymers.[29] The final dataset contains a diverse range of polymer backbones including polystyrenes, polyacrylates, and polyurethanes. A detailed breakdown is provided in B.2.

2.1.2 Fluoropolymers

Fluoropolymers are a critical class of polymers that fall within the broader class of materials known as polyfluoroalkyl substances (PFAS). PFAS materials have recently gained significant attention due to their

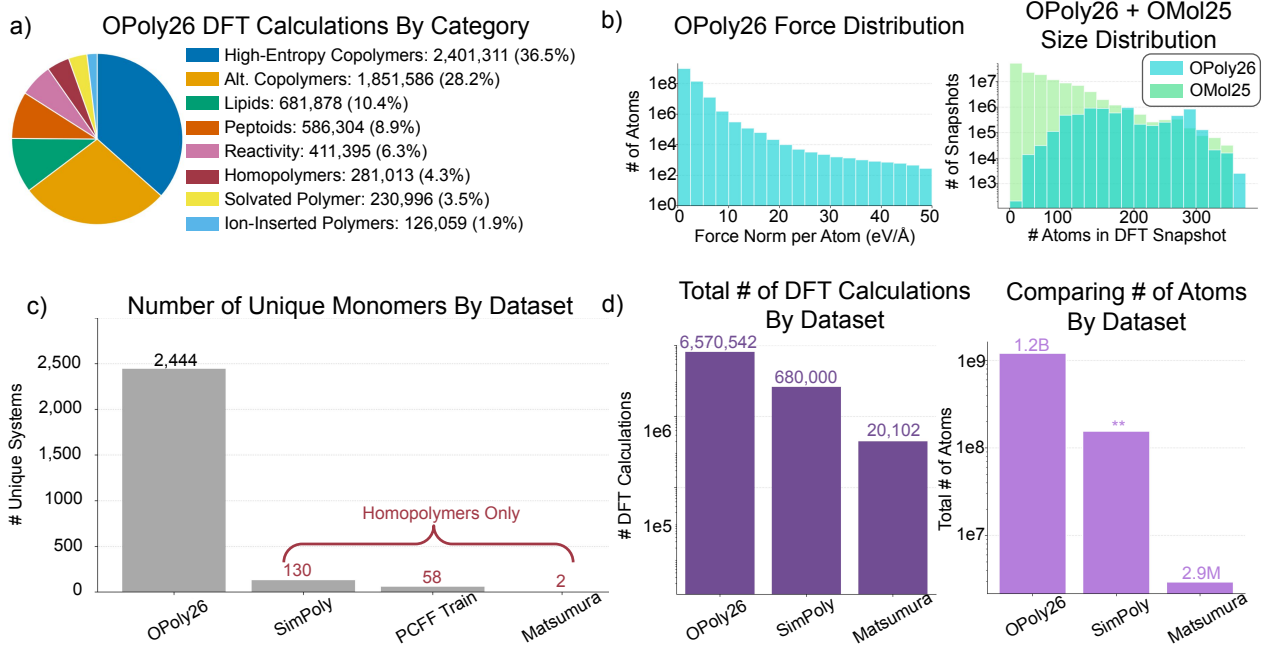


Figure 2 Summary of OPoly26 dataset statistics. a) Distribution of OPoly26 DFT calculations by polymer categories. b) Distribution of force norms per atom across all OPoly26 DFT calculations (left) and distribution of the number of atoms in each OPoly26 DFT calculation in comparison to OMol25 (right). c) Comparison of the number of unique monomers across polymer datasets. d) Total number of atoms contained in polymer DFT datasets meant for MLIP training including OPoly26, data from SimPoly[26], and the work of Matsumura et al.[25]. **As SimPoly is not yet publicly available, we estimate the total number of atoms by assuming the highest possible number of atoms in each DFT calculation.

widespread usage in consumer products, coupled with their extreme persistence in the human body and environment as well as significant human health risks [30, 31]. Due to the lack of open datasets of experimentally synthesized fluoropolymers, we instead extract fluoropolymer compositions from the Open Macromolecular Genome (OMG) of ML-generated polymer systems that are compatible with known polymerization reactions [32]. To ensure a diverse range of fluoropolymer chemistries are represented, we evenly sample fluorinated compositions from the 17 polymerization reactions described in OMG.

2.1.3 Optical Polymers

Polymers with π -conjugated backbones possess unique optical and electronic properties [33]. As a result, conjugated polymers are important to a wide range of innovative optical technologies including photocatalysts, organic solar cells, photovoltaics, and organic light-emitting diodes [34–36]. We sample optical polymer systems from the Polymer Chempop dataset [10], which spans the space of 892 monomers originally defined by Bai et al. [34].

2.1.4 Polymer Electrolytes

Solid-phase polymer electrolytes are being widely explored as replacements to currently used liquid electrolytes in lithium-ion batteries due to their improved safety (i.e. lower volatility and flammability) coupled with their ease of thin-film processing.[3, 37–39] In OPoly26, we include 300 diverse polymer compositions (without ions) from the PolyGen dataset of amorphous polymer electrolytes.[37–39] To ensure that we appropriately capture the interactions between polymer chains and ionic species, we also create ion-inserted polymer systems, described in Section B.6

2.1.5 Peptoids

Peptoids are synthetic biopolymers that consist of N-substituted glycines. Importantly, this chemical structure of peptoids allows for a wide array of side-chain chemistries to be incorporated into the peptoid structure, thereby allowing for the systematic design and tailoring of material properties. Our catalog of peptoid monomers is comprised of experimentally synthesized, charge-neutral peptoid monomers from the Peptoid Data Bank,[40] as well as hand-collected peptoid monomers that are of particular interest for peptoid-based EUV lithography photoresists.[41]

2.1.6 Lipids

Lipids, although not polymeric in nature, are included in OPoly26 because lipid simulations suffer from many of the same challenges as polymer simulations. Lipids are a larger class of hydrophobic/amphipathic biomolecules that are insoluble in water. Many lipids spontaneously form supramolecular assemblies, such as bilayers, in aqueous environments, and the material properties of these superstructures are defined by the specific lipid composition and detailed environmental conditions.[42] Capturing lipid bilayer properties in simulations can be challenging and often requires integrating over several length and time scales [43, 44]. To span a diverse set of common lipids in different bilayer environments, we sample lipid simulation snapshots from the NMRlipid database [45].

2.2 Polymer Architectures

We strive to maximize structural and interaction diversity spanned by OPoly26 to enhance the generalizability of MLIPs trained on the dataset while ensuring that polymer structures are computationally feasible to simulate. As outlined in Table 1, we generate bulk, amorphous cells of the polymeric structures with the RadonPy package[27], where chain architectures are limited to linear homopolymers and copolymers (including alternating and random). Additionally, we perform MD simulations of alternating copolymers in the presence of 17 different explicit solvent environments (Appendix C.2.2). To increase structural and interaction diversity, we also generate high-entropy copolymers, which are random copolymers consisting of between 4-10 distinct monomers, where the monomers are sampled from all polymer compositions in Sections 2.1.1-2.1.4. Peptoids are sampled in a similar manner but with a small amount of water also present.

2.3 Simulating Polymer Dynamics

The combination of the polymer compositions (Section 2.1) with the polymer architectures (Section 2.2) results in the creation of 94k unique amorphous polymer simulation cells (see Table 1). Next, we employ a variety of simulation strategies (MD, MLIP-MD, AFIR, and DFTB) to yield a rich dataset of polymer conformations for MLIP training and testing (Figure 3).

Table 1 Summary of input structures to the OPoly26 MD-based data generation.

Category Name	Compositions	# MD Trajectories	Cell Description
300 Atom Homopolymers	Fluoro, Trad., Optical, Electrolytes	2,155	3 chains of 100 atom homopolymers
5000 Atom Homopolymers	Fluoro, Trad., Optical, Electrolytes	2,046	10 chains of 500 atom homopolymers
300 Atom Copolymers	Fluoro, Trad., Optical, Electrolytes	17,017	2 chains of 150 atom alternating copolymers
5000 Atom Copolymers	Fluoro, Trad., Optical, Electrolytes	16,247	10 chains of 500 atom alternating copolymers
300 Atom High-Entropy Copolymers	High-Entropy Copolymers	17,434	3 chains of 100 atom random polymers with between 3-6 unique comonomers
5000 Atom High-Entropy Copolymers	High-Entropy Copolymers	19,622	10 chains of 500 atom random polymers with between 5-10 unique comonomers
5000 Atom Solvated Copolymers	Fluoro, Trad., Optical, Electrolytes	8,383	1 chain of 500 atom random copolymer with 4500 solvent atoms
300 Atom Peptoids	Peptoids	6,570	3 chains of 100 atom high-entropy copolymers with 10 water molecules
5000 Atom Peptoids	Peptoids	4,962	10 chains of 300 atom high-entropy copolymers with 100 water molecules

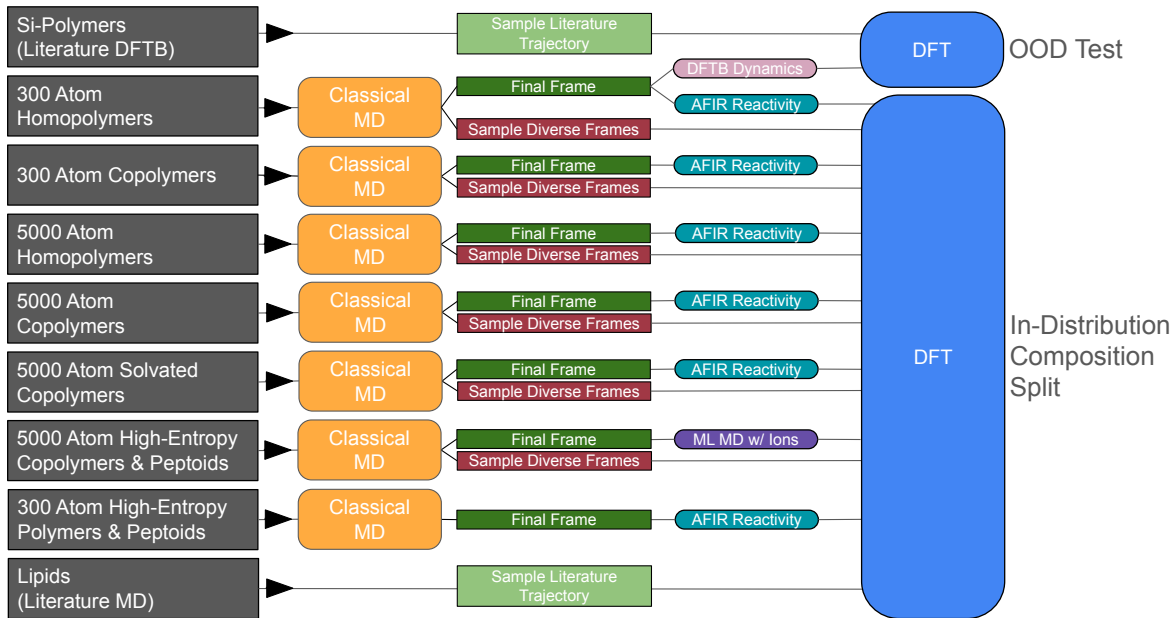


Figure 3 Overview of the OPoly26 data generation process. Starting from a diverse collection of polymeric compositions (Section 2.1), we apply a sequence of computational steps tailored to each class of materials. In general, we first use classical MD simulations to generate a broad distribution of polymer configurations (Section 2.3). From these trajectories, we sample both the relaxed final frame (for use in further calculations) as well as sample diverse frames from across the MD trajectory, as described in Section 2.5. All resulting structures are subsequently passed into a final DFT calculation, yielding the MLIP training and test data.

To generate large quantities of polymer structures, we carried out a series of classical all-atom MD simulations using the LAMMPS MD suite[46] and the RadonPy tools made available by Hayashi et al.[27] Additional details of our MD procedure are provided in Appendix C. The final frames of high-entropy copolymers and peptoids further had ions inserted into voids and were then subjected to MLIP-MD simulations. Additional details are provided in Appendix C.4. Finally, homopolymer final frames were subjected to density functional tight binding (DFTB) simulations to generate a set of distinct configurations for an out-of-distribution test set. Additional details are provided in Appendix C.5.

2.4 Reactivity

To probe polymer-specific reactivity under realistic, condensed-phase environments, we generate reactive configurations through single-ended artificial force-induced reaction (AFIR)[47, 48] searches that target bond dissociation events within polymer chains. AFIR trajectories, which serve to approximate the minimum energy pathway between reactants and their products, are initialized from a converged MD trajectory frame resulting from Section 2.3. Bond dissociations in polymer systems are important for the study of thermal, photochemical, and mechanical degradation as well as reversible and living polymerizations, but also serve as a facile way to explore polymer reactivity across various monomer and co-monomer compositions. Additional details are provided in Appendix D.

2.5 Extracting Polymer Substructures from Trajectories

Due to the large computational expense of DFT calculations, it is infeasible to perform single point DFT calculations on entire 5000 atom polymer simulation cells. Instead, we extract smaller substructures (<360 atoms) from the 5000 atom polymer simulation cells to capture a diversity of local chemical environments. From each MD trajectory, we intentionally sample a high proportion of frames from the simulated annealing

portion, resulting in preferential sampling of non-equilibrium polymer structures (as seen in Figure 2 force distribution). To further aid in sampling diverse configurations within each trajectory, we sample frames of the trajectory with the largest dissimilarity to all other structures in the trajectory. Finally, structures suitable for molecular DFT are created by extracting hydrogen-capped shells of atoms, terminating between polymer repeat units. Our detailed procedure for extracting lipid and polymeric substructures is detailed in Appendix E.

2.6 DFT Calculation Details

All DFT calculations are performed at the level of theory described in full detail in OMol25[24]. Specifically, we employ the triple-zeta def2-TZVPD basis set[49] and the range-separated hybrid meta-GGA DFT functional ω B97M-V[50] due to its performance as one of the most accurate functionals across various DFT functional benchmarks.[51] Complete details are provided in Appendix A.

2.7 OPoly26 Training, Validation, and Test Splits

OPoly26 is divided into consistent training, validation, and test splits consisting of 6,099,878, 210,924, and 259,740 polymer substructures, respectively, based on the atomic composition of each datapoint. As an additional out-of-distribution (OOD) test split, we use the **DFTB** generated structures as detailed in Section C.5. Notably, this DFTB test split is OOD with respect to the main train split in terms of both the simulation method used and the temperature of the simulations (600 K). We perform an additional OOD test evaluation on a **Si-polymers** dataset of silicone polymers undergoing radiation-induced degradation processes.[52] While this Si-polymers test set cannot be used with MLIP models trained on OPoly26 alone, as there is no silicon in the training data, it can be used with models trained on OMol25 or on both OPoly26 and OMol25.

2.8 Dataset Limitations

With more than 6 million high-accuracy DFT calculations, OPoly26 is the largest and most comprehensive dataset for training MLIP models on non-biological polymers to date. Nevertheless, given the broad usage of the term “polymer”, it is important to specifically outline classes of polymeric materials that are not explicitly covered by OPoly26. First, OPoly26 does not contain gradient copolymers, block copolymers, branched polymers, crosslinked polymers or graft polymers, as these polymer chain architectures cannot be appropriately represented in our <360 atom DFT simulation cells. Nevertheless, given the common local chemical environments between these unseen polymer architectures are those present in OPoly26, future work will explore how MLIPs trained on OPoly26 can generalize to these out-of-distribution polymer architectures. We also note that OPoly26 does not include any silicon or other heavy p-block element-containing polymers. Finally, although all monomer compositions have been verified for chemical validity, not all monomer compositions nor polymer architectures present in OPoly26 are guaranteed to be synthesizable (see Appendix B).

3 Evaluations

We are in the process of finalizing a set of evaluation tasks that are designed to assess the performance of models trained on OPoly26 to accurately capture local polymer structures and their interactions with nearby chemical moieties. This manuscript will be updated with additional details and results on these evaluations in the near future.

4 Baseline Models

To establish a set of baseline results, we evaluate the performance of eSEN models[53] trained on OMol25, OPoly26, and OMol25 + OPoly26. We note that the primary focus of this work is not to evaluate a comprehensive list of MLIP training procedures, but to explore how training on different combinations of small molecule and polymer data improves the downstream model performance in these different domains. Note that models are trained in a step equivalent manner. Models trained on both OPoly26 and OMol25 have

seen the same total amount of data points as OPoly26 only or OMol25 only and therefore have seen any given OPoly26 or OMol25 data point less than the solo-trained models.

5 Results

By comparing OPoly26 test set performance of models trained on only OMol25, only OPoly26, and OMol25 + OPoly26, we seek to probe the benefit of polymer-specific training data versus more general molecular data for polymer-specific MLIP prediction tasks - and whether the addition of polymer-specific data degrades performance in other chemical domains. Future work will explore model performance on both additional DFT-calculated evaluation tasks and experimentally measured bulk polymer properties.

Table 2 Summary of energy and force prediction performance on OPoly26 test splits of models trained on different training datasets. For each model, we report the mean absolute error in total energy (meV) and forces (meV/Å). For test and val compositions, models trained on OPoly26 have substantially reduced energy error compared with a model trained only on OMol25, while a model trained on both OMol25 and OPoly26 has the lowest force error. The Si-polymer test set has substantially larger energy errors, and while the addition of OPoly26 data does meaningfully reduce energy error, the reduction is not as substantial as for val/test. In contrast, all models have low error on the DFTB test set, and OPoly26 data does not improve performance. Note that models are trained in a step equivalent manner so models trained on both OPoly26 and OMol25 have seen a given training data point fewer times than solo-trained models.

Train Dataset	Test Composition		Val Composition		DFTB		Si-Polymers	
	Energy MAE↓	Force MAE↓	Energy MAE↓	Force MAE↓	Energy MAE↓	Force MAE↓	Energy MAE↓	Force MAE↓
OMol25 Only	78.3	6.5	68.2	6.2	30.0	3.8	184.2	5.3
OPoly26 Only	29.7	5.7	28.8	5.4	31.2	4.5	—	—
OPoly26 + OMol25	32.7	5.2	31.4	5.0	30.8	4.0	160.4	6.0

Energy MAE(meV), Force MAE(meV/Å)

We find that polymer specific data is necessary to obtain sub-kcal/mol total energy accuracy ("chemical accuracy" = 1 kcal/mol = 43 meV) on diverse polymer structures (Table 2). Specifically, the OPoly26 and OPoly26 + OMol25 model shows less than half the total energy mean absolute error (MAE) of a model trained only on OMol25 in test and val compositional splits. However, atomic force MAE only slightly improves, perhaps due to the fact that force errors on the OPoly26 splits for the OMol25-only model are already quite small. The Si-polymer set presents a substantially more challenging test, featuring high-energy systems far from equilibrium generated under simulated irradiation conditions of silicon polymers. Neither simulated irradiated systems nor silicon polymers are present in either the OPoly26 training set or OMol25. These structures result in much higher energy errors than test or val compositions (though still practically useful for simulations). Interestingly, the OPoly26 + OMol25 model has ~15% lower energy error compared with the OMol25-only model, demonstrating that organic polymer data holds some value for non-carbon-based polymers. Finally, all three models perform similarly, and with quite low errors, on the DFTB test set, perhaps because only the DFTB set samples solely homopolymers.

Table 3 Summary of model performances on OMol25 evaluation. Evaluation details are provided in the OMol25 paper.[24] Models trained on only OMol25 or OPoly26 + OMol25 perform comparably, demonstrating that the addition of polymer-specific data does not degrade performance in other chemical domains. A model trained solely on OPoly26 performs worse on or cannot reasonably perform tasks due to insufficient elemental/charge/spin coverage. Note that models are trained in a step equivalent manner so models trained on both OPoly26 and OMol25 have seen a given training data point fewer times than solo-trained models.

Train Dataset	Ligand strain	Conformers	Protonation	Protein-Ligand	IE/EA	Spin gap					
	Strain energy MAE /meV/↓	RMSD min. /Å /↓	RMSD ensemble /Å /↓	Δ Energy MAE /meV/↓	Δ Energy MAE /meV/↓	Ixn Energy MAE /meV/↓	Ixn Forces MAE /meV/Å /↓	Δ Energy MAE /meV/↓	Δ Forces MAE /meV/Å /↓	Δ Energy MAE /meV/↓	Δ Forces MAE /meV/Å /↓
OPoly26 Only	17.6	0.32	0.06	10.2	—	—	—	—	—	—	—
OMol25 Only	4.18	0.21	0.03	4.55	0.05	30.2	166.3	4.41	216.4	55.1	316.4
OPoly26 + OMol25	5.09	0.20	0.04	5.26	0.06	27.3	191.9	4.85	209.2	55.1	311.0

As seen in Table 3, the addition of OPoly26 data atop OMol25 data does not result in any significant degradation of performance on the OMol25 evaluations. The common level of theory of these two datasets and the complementary nature of the data accommodate broad performance with expressive models. However, a model trained only on OPoly26 does not contain comparable broad molecular chemical diversity or elemental/charge/spin distribution to OMol25 and so performs worse on or is inapplicable to many general molecular evaluation tasks.

6 Conclusions and future directions

Open Polymers 2026 (OPoly26) is the first large-scale open-source DFT dataset for MLIP training with a diverse range of synthetic polymer systems including linear copolymers, solvated polymers and reactive polymer structures. We show that models trained on OPoly26 and OMol25 have small errors versus reference DFT for both small molecule and polymer system predictions without the need for system-specific fitting. Further, OPoly26 data markedly improves model polymer energy predictions compared with models trained only on broad molecular data (i.e. OMol25) without causing any significant performance degradation on molecular prediction tasks in other domains. Additional analysis is currently underway to elucidate how performance improvements from OPoly26 are distributed across polymer categories as well as how OPoly26 data impacts model performance on specific chemical domains covered by OMol25. We are also finalizing a set of evaluations that seek to assess a model’s ability to accurately predict local polymer structures and their interactions with nearby chemical moieties, with respect to DFT, to shed light on areas where future MLIP model architectures could meaningfully improve. Finally, we plan to examine how OPoly26 data impacts the capacity of models trained on OPoly26 to predict experimentally measured bulk polymer properties, leveraging the curated data in SimPoly.

By enhancing MLIP performance across polymer domains, we envision that OPoly26 could enable accurate atomistic simulations of polymer dynamics and reactivity, facilitating computational study of polymer membranes for fuel cells and separations, polymer degradation pathways and upcycling, and polymer synthesis with minimal up-front burden for users. To foster community engagement and accelerate the development of generalizable polymer models, we release the OPoly26 dataset with an open-source CC-BY-4.0 license at <https://huggingface.co/facebook/OMol25> and will update the OMol25 leaderboard with polymer-centric tests and evaluations in the near future.

7 Acknowledgments

E.R.A. acknowledges support from the Laboratory Directed Research and Development Program of Lawrence Livermore National Laboratory, project number LDRD 24-SI-008. E.R.A. also acknowledges the support of

the Livermore Computing staff. N.L., J.D., S. S. M., and M.P.K. acknowledge support from the Laboratory Directed Research and Development Program of Lawrence Livermore National Laboratory, project number LDRD 23-ERD-030. This work was produced under the auspices of the U.S. Department of Energy by Lawrence Livermore National Laboratory under Contract DE-AC52-07NA27344.

L.C. acknowledges support by the U.S. Department of Energy, Office of Science, Office of Advanced Scientific Computing Research, Department of Energy Computational Science Graduate Fellowship under Award Number DE-SC0024386.

N.K. and S.M.B. acknowledge support from the Center for High Precision Patterning Science (CHiPPS), an Energy Frontier Research Center funded by the U.S. Department of Energy, Office of Science, Basic Energy Sciences at Lawrence Berkeley National Laboratory under Contract No. DE-AC02-34205CH11231.

8 Data availability

The OPoly26 dataset is released under a CC-BY-4.0 license at <https://huggingface.co/facebook/OMol25> and code is available at <https://github.com/facebookresearch/fairchem>.

References

- [1] Sangroniz, A.; Zhu, J.-B.; Tang, X.; Etxeberria, A.; Chen, E. Y.-X.; Sardon, H. Packaging materials with desired mechanical and barrier properties and full chemical recyclability. *Nature Communications* **2019**, *10*, 3559.
- [2] Ligon, S. C.; Liska, R.; Stampfl, J.; Gurr, M.; Mülhaupt, R. Polymers for 3D Printing and Customized Additive Manufacturing. *Chemical Reviews* **2017**, *117*, 10212–10290.
- [3] Song, Z.; Chen, F.; Martínez-Ibañez, M.; Feng, W.; Forsyth, M.; Zhou, Z.; Armand, M.; Zhang, H. A reflection on polymer electrolytes for solid-state lithium metal batteries. *Nature Communications* **2023**, *14*, 4884.
- [4] Jambeck, J. R.; Geyer, R.; Wilcox, C.; Siegler, T. R.; Perryman, M.; Andrade, A.; Narayan, R.; Law, K. L. Plastic waste inputs from land into the ocean. *Science* **2015**, *347*, 768–771.
- [5] Li, Y.; Tao, L.; Wang, Q.; Wang, F.; Li, G.; Song, M. Potential Health Impact of Microplastics: A Review of Environmental Distribution, Human Exposure, and Toxic Effects. *Environment & Health* **2023**, *1*, 249–257.
- [6] Song, P.; Wang, H. High-Performance Polymeric Materials through Hydrogen-Bond Cross-Linking. *Advanced Materials* **2020**, *32*, 1901244.
- [7] Xie, Z.; Hu, B.-L.; Li, R.-W.; Zhang, Q. Hydrogen Bonding in Self-Healing Elastomers. *ACS Omega* **2021**, *6*, 9319–9333.
- [8] Chen, J.; Li, L.; Luo, J.; Meng, L.; Zhao, X.; Song, S.; Demchuk, Z.; Li, P.; He, Y.; Sokolov, A. P.; Cao, P.-F. Covalent adaptable polymer networks with CO₂-facilitated recyclability. *Nature Communications* **2024**, *15*, 6605.
- [9] Gartner, T. E. I.; Jayaraman, A. Modeling and Simulations of Polymers: A Roadmap. *Macromolecules* **2019**, *52*, 755–786.
- [10] Aldeghi, M.; Coley, C. W. A graph representation of molecular ensembles for polymer property prediction. *Chemical Science* **2022**, *13*.
- [11] Melenkevitz, J.; Muthukumar, M. Density functional theory of lamellar ordering in diblock copolymers. *Macromolecules* **1991**, *24*, 4199–4205.
- [12] Gooneie, A.; Schuschnigg, S.; Holzer, C. A Review of Multiscale Computational Methods in Polymeric Materials. *Polymers* **2017**, *9*, 16, Publisher: Multidisciplinary Digital Publishing Institute.
- [13] Bishop, M.; Kalos, M. H.; Frisch, H. L. Molecular dynamics of polymeric systems. *The Journal of Chemical Physics* **1979**, *70*, 1299–1304.
- [14] Sun, H.; Mumby, S. J.; Maple, J. R.; Hagler, A. T. An ab Initio CFF93 All-Atom Force Field for Polycarbonates. *Journal of the American Chemical Society* **1994**, *116*, 2978–2987.
- [15] Sun, H. COMPASS: An ab Initio Force-Field Optimized for Condensed-Phase ApplicationsOverview with Details on Alkane and Benzene Compounds. *The Journal of Physical Chemistry B* **1998**, *102*, 7338–7364.
- [16] Jorgensen, W. L.; Maxwell, D. S.; Tirado-Rives, J. Development and Testing of the OPLS All-Atom Force Field on Conformational Energetics and Properties of Organic Liquids. *Journal of the American Chemical Society* **1996**, *118*, 11225–11236, Publisher: American Chemical Society.
- [17] Kaminski, G. A.; Friesner, R. A.; Tirado-Rives, J.; Jorgensen, W. L. Evaluation and Reparametrization of the OPLS-AA Force Field for Proteins via Comparison with Accurate Quantum Chemical Calculations on Peptides. *The Journal of Physical Chemistry B* **2001**, *105*, 6474–6487, Publisher: American Chemical Society.
- [18] Mayo, S. L.; Olafson, B. D.; Goddard, W. A. DREIDING: a generic force field for molecular simulations. *The Journal of Physical Chemistry* **1990**, *94*, 8897–8909, Publisher: American Chemical Society.
- [19] Wood, B. M. et al. UMA: A Family of Universal Models for Atoms. 2025; <https://arxiv.org/abs/2506.23971>.
- [20] Rhodes, B.; Vandenhaut, S.; Šimkus, V.; Gin, J.; Godwin, J.; Duignan, T.; Neumann, M. Orb-v3: atomistic simulation at scale. 2025; arXiv:2504.06231 [cond-mat].
- [21] Batatia, I.; Kovács, D. P.; Simm, G. N. C.; Ortner, C.; Csányi, G. MACE: Higher Order Equivariant Message Passing Neural Networks for Fast and Accurate Force Fields. 2023; arXiv:2206.07697 [stat].
- [22] Chiang, Y.; Kreiman, T.; Zhang, C.; Kuner, M. C.; Weaver, E.; Amin, I.; Park, H.; Lim, Y.; Kim, J.; Chrzan, D.; Walsh, A.; Blau, S. M.; Asta, M.; Krishnapriyan, A. S. MLIP Arena: Advancing Fairness and Transparency in

Machine Learning Interatomic Potentials via an Open, Accessible Benchmark Platform. 2025; arXiv:2509.20630 [physics].

- [23] Yuan, E. C. Y.; Liu, Y.; Chen, J.; Zhong, P.; Raja, S.; Kreiman, T.; Vargas, S.; Xu, W.; Head-Gordon, M.; Yang, C.; Blau, S. M.; Cheng, B.; Krishnapriyan, A.; Head-Gordon, T. Foundation Models for Atomistic Simulation of Chemistry and Materials. 2025.
- [24] Levine, D. S. et al. The Open Molecules 2025 (OMol25) Dataset, Evaluations, and Models. 2025.
- [25] Matsumura, N.; Yoshimoto, Y.; Yamazaki, T.; Amano, T.; Noda, T.; Ebata, N.; Kasano, T.; Sakai, Y. Generator of Neural Network Potential for Molecular Dynamics: Constructing Robust and Accurate Potentials with Active Learning for Nanosecond-Scale Simulations. *Journal of Chemical Theory and Computation* **2025**, *21*, 3832–3846.
- [26] Simm, G. N. C. et al. SimPoly: Simulation of Polymers with Machine Learning Force Fields Derived from First Principles. 2025; <http://arxiv.org/abs/2510.13696>, arXiv:2510.13696 [physics].
- [27] Hayashi, Y.; Shiomi, J.; Morikawa, J.; Yoshida, R. RadonPy: automated physical property calculation using all-atom classical molecular dynamics simulations for polymer informatics. *npj Computational Materials* **2022**, *8*, 222.
- [28] Otsuka, S.; Kuwajima, I.; Hosoya, J.; Xu, Y.; Yamazaki, M. PoLyInfo: Polymer Database for Polymeric Materials Design. 2011 International Conference on Emerging Intelligent Data and Web Technologies. 2011; pp 22–29.
- [29] Bicerano, J. *Prediction of Polymer Properties*, 3rd ed.; CRC Press: Boca Raton, 2002.
- [30] Lohmann, R.; Cousins, I. T.; DeWitt, J. C.; Glüge, J.; Goldenman, G.; Herzke, D.; Lindstrom, A. B.; Miller, M. F.; Ng, C. A.; Patton, S.; Scheringer, M.; Trier, X.; Wang, Z. Are Fluoropolymers Really of Low Concern for Human and Environmental Health and Separate from Other PFAS? *Environmental Science & Technology* **2020**, *54*, 12820–12828.
- [31] eBioMedicine Forever chemicals: the persistent effects of perfluoroalkyl and polyfluoroalkyl substances on human health. *eBioMedicine* **2023**, *95*.
- [32] Kim, S.; Schroeder, C. M.; Jackson, N. E. Open Macromolecular Genome: Generative Design of Synthetically Accessible Polymers. *ACS Polymers Au* **2023**, *3*, 318–330.
- [33] Rasmussen, S. C.; Gilman, S. J.; Wilcox, W. D. *Conjugated Polymers: Synthesis & Design*; American Chemical Society: Washington, DC, USA, 2023.
- [34] Bai, Y.; Wilbraham, L.; Slater, B. J.; Zwijnenburg, M. A.; Sprick, R. S.; Cooper, A. I. Accelerated Discovery of Organic Polymer Photocatalysts for Hydrogen Evolution from Water through the Integration of Experiment and Theory. *Journal of the American Chemical Society* **2019**, *141*, 9063–9071.
- [35] Zhang, T.; An, C.; Bi, P.; Lv, Q.; Qin, J.; Hong, L.; Cui, Y.; Zhang, S.; Hou, J. A Thiadiazole-Based Conjugated Polymer with Ultradeep HOMO Level and Strong Electroluminescence Enables 18.6% Efficiency in Organic Solar Cell. *Advanced Energy Materials* **2021**, *11*, 2101705.
- [36] Xu, Y.; Cui, Y.; Yao, H.; Zhang, T.; Zhang, J.; Ma, L.; Wang, J.; Wei, Z.; Hou, J. A New Conjugated Polymer that Enables the Integration of Photovoltaic and Light-Emitting Functions in One Device. *Advanced Materials* **2021**, *33*, 2101090.
- [37] Xie, T.; France-Lanord, A.; Wang, Y.; Lopez, J.; Stolberg, M. A.; Hill, M.; Leverick, G. M.; Gomez-Bombarelli, R.; Johnson, J. A.; Shao-Horn, Y.; Grossman, J. C. Accelerating amorphous polymer electrolyte screening by learning to reduce errors in molecular dynamics simulated properties. *Nature Communications* **2022**, *13*, 3415.
- [38] Lei, X.; Ye, W.; Yang, Z.; Schweigert, D.; Kwon, H.-K.; Khajeh, A. A self-improvable Polymer Discovery Framework Based on Conditional Generative Model. *arXiv preprint arXiv:2312.04013* **2023**,
- [39] Yang, Z.; Ye, W.; Lei, X.; Schweigert, D.; Kwon, H.-K.; Khajeh, A. De novo design of polymer electrolytes with high conductivity using gpt-based and diffusion-based generative models. *arXiv preprint arXiv:2312.06470* **2023**,
- [40] Eastwood, J. R. B.; Weisberg, E. I.; Katz, D.; Zuckermann, R. N.; Kirshenbaum, K. Guidelines for designing peptoid structures: Insights from the Peptoid Data Bank. *Peptide Science* **2023**, *115*, e24307.
- [41] Adams, C. P.; Henein, C.; Meng, X.; Yuan, C.; Read de Alaniz, J.; Ober, C. K.; Segalman, R. A. Polymer Sequence Alters Sensitivity and Resolution in Chemically Amplified Polypeptoid Photoresists. *ACS Macro Letters* **2025**, *14*, 1055–1059.

- [42] Vattulainen, I.; Rog, T. Lipid Simulations: A Perspective on Lipids in Action. *Cold Spring Harbor Perspectives in Biology* **2011**, *3*, a004655.
- [43] Enkavi, G.; Javanainen, M.; Kulig, W.; Rog, T.; Vattulainen, I. Multiscale Simulations of Biological Membranes: The Challenge To Understand Biological Phenomena in a Living Substance. *Chem Rev* **2019**, *119*, 5607–5774.
- [44] Marrink, S. J.; Corradi, V.; Souza, P. C. T.; Ingólfsson, H. I.; Tieleman, D. P.; Sansom, M. S. P. Computational Modeling of Realistic Cell Membranes. *Chemical Reviews* **2019**, *119*, 6184–6226.
- [45] Kiirikki, A. M. et al. Overlay databank unlocks data-driven analyses of biomolecules for all. *Nature Communications* **2024**, *15*, 1136.
- [46] Thompson, A. P.; Aktulga, H. M.; Berger, R.; Bolintineanu, D. S.; Brown, W. M.; Crozier, P. S.; int Veld, P. J.; Kohlmeyer, A.; Moore, S. G.; Nguyen, T. D.; others LAMMPS-a flexible simulation tool for particle-based materials modeling at the atomic, meso, and continuum scales. *Computer Physics Communications* **2022**, *271*, 108171.
- [47] Maeda, S.; Harabuchi, Y.; Takagi, M.; Taketsugu, T.; Morokuma, K. Artificial Force Induced Reaction (AFIR) Method for Exploring Quantum Chemical Potential Energy Surfaces. *The Chemical Record* **2016**, *16*, 2232–2248.
- [48] Levine, D. S.; Jacobson, L. D.; Bochevarov, A. D. Large Computational Survey of Intrinsic Reactivity of Aromatic Carbon Atoms with Respect to a Model Aldehyde Oxidase. *Journal of Chemical Theory and Computation* **2023**, *19*, 9302–9317, Publisher: American Chemical Society.
- [49] Weigend, F.; Ahlrichs, R. Balanced basis sets of split valence, triple zeta valence and quadruple zeta valence quality for H to Rn: Design and assessment of accuracy. *Physical Chemistry Chemical Physics* **2005**, *7*, 3297–3305.
- [50] Mardirossian, N.; Head-Gordon, M. ω B97M-V: A combinatorially optimized, range-separated hybrid, meta-GGA density functional with VV10 nonlocal correlation. *The Journal of Chemical Physics* **2016**, *144*, 214110.
- [51] Mardirossian, N.; Head-Gordon, M. Thirty years of density functional theory in computational chemistry: an overview and extensive assessment of 200 density functionals. *Molecular Physics* **2017**, *115*, 2315–2372.
- [52] Kroonblawd, M.; Goldman, N.; Maiti, A.; Lewicki, J. Polymer degradation through chemical change: a quantum-based test of inferred reactions in irradiated polydimethylsiloxane. **2022**,
- [53] Fu, X.; Wood, B. M.; Barroso-Luque, L.; Levine, D. S.; Gao, M.; Dzamba, M.; Zitnick, C. L. Learning Smooth and Expressive Interatomic Potentials for Physical Property Prediction. 2025; <http://arxiv.org/abs/2502.12147>, arXiv:2502.12147 [physics].
- [54] Neese, F. Software Update: The ORCA Program System—Version 6.0. *WIREs Computational Molecular Science* **2025**, *15*, e70019.
- [55] RDKit community RDKit: Open-source cheminformatics. <https://www.rdkit.org>, 2025.
- [56] Ramsundar, B.; Eastman, P.; Walters, P.; Pande, V.; Leswing, K.; Wu, Z. *Deep Learning for the Life Sciences*; 2019.
- [57] Richard J. Gowers; Max Linke; Jonathan Barnoud; Tyler J. E. Reddy; Manuel N. Melo; Sean L. Seyler; Jan Domański; David L. Dotson; Sébastien Buchoux; Ian M. Kenney; Oliver Beckstein MDAnalysis: A Python Package for the Rapid Analysis of Molecular Dynamics Simulations. Proceedings of the 15th Python in Science Conference. 2016; pp 98 – 105.
- [58] Abbott, L. J.; Hart, K. E.; Colina, C. M. Polymatic: a generalized simulated polymerization algorithm for amorphous polymers. *Theoretical Chemistry Accounts* **2013**, *132*, 1334.
- [59] Wang, J.; Wolf, R. M.; Caldwell, J. W.; Kollman, P. A.; Case, D. A. Development and testing of a general amber force field. *Journal of Computational Chemistry* **2004**, *25*, 1157–1174.
- [60] Träg, J.; Zahn, D. Improved GAFF2 parameters for fluorinated alkanes and mixed hydro- and fluorocarbons. *Journal of Molecular Modeling* **2019**, *25*, 39.
- [61] Bayly, C. I.; Cieplak, P.; Cornell, W.; Kollman, P. A. A well-behaved electrostatic potential based method using charge restraints for deriving atomic charges: the RESP model. *The Journal of Physical Chemistry* **1993**, *97*, 10269–10280.
- [62] Price, D. J.; Brooks, C. L., III A modified TIP3P water potential for simulation with Ewald summation. *The Journal of Chemical Physics* **2004**, *121*, 10096–10103.

- [63] Martínez, L.; Andrade, R.; Birgin, E. G.; Martínez, J. M. PACKMOL: A package for building initial configurations for molecular dynamics simulations. *Journal of computational chemistry* **2009**, *30*, 2157–2164.
- [64] Larsen, A. H. et al. The Atomic Simulation Environment—A Python library for working with atoms. *Journal of Physics: Condensed Matter* **2017**, *29*, 273002.
- [65] Gaus, M.; Cui, Q.; Elstner, M. DFTB3: Extension of the Self-Consistent-Charge Density-Functional Tight-Binding Method (SCC-DFTB). *Journal of Chemical Theory and Computation* **2011**, *7*, 931–948.
- [66] Hourahine, B. et al. DFTB+, a software package for efficient approximate density functional theory based atomistic simulations. *The Journal of Chemical Physics* **2020**, *152*, 124101.
- [67] Gaus, M.; Lu, X.; Elstner, M.; Cui, Q. Parameterization of DFTB3/3OB for Sulfur and Phosphorus for Chemical and Biological Applications. *Journal of Chemical Theory and Computation* **2014**, *10*, 1518–1537.
- [68] Mermin, N. D. Thermal Properties of the Inhomogeneous Electron Gas. *Physical Review* **1965**, *137*, A1441–A1443.
- [69] Taylor, M. G.; Burrill, D. J.; Janssen, J.; Batista, E. R.; Perez, D.; Yang, P. Architector for high-throughput cross-periodic table 3D complex building. *Nature Communications* **2023**, *14*, 2786.

Appendix

Appendix Table of Contents

A Calculation Details	16
A.1 Calculation Quality Filters	16
A.2 Computed Properties	16
B Polymer Compositions	17
B.1 General Sanitization	17
B.2 Traditional Polymers	17
B.3 Fluoropolymers	17
B.4 Optical Polymers	18
B.5 Polymer Electrolytes	19
B.6 Ion-Inserted Polymers	19
B.6.1 Lipids	19
B.7 Polymer Architectures	20
C MD Details	20
C.1 MD Force Field	20
C.2 System Preparation	21
C.2.1 Preparation of Bulk (Amorphous) Polymer Cells	21
C.2.2 Preparation of Solvated (Infinite Dilution) Polymer Cells	23
C.3 Solvents	23
C.4 Ion insertion MLIP-MD	25
C.5 DFTB	26
D Reactivity	26
D.1 AFIR Preparation	26
D.1.1 Bond Selection	26
D.1.2 Pre-Trimming	27
D.1.3 Charge Diversification	27
D.2 AFIR Protocol	28
D.3 Post-Trimming	29
E Extracting Substructures from Trajectories	29
E.1 Polymers	29
E.2 Lipids	29

A Calculation Details

All calculations in OPoly26 were carried out with the ORCA 6.0.0 DFT package [54]. ORCA supports various integral acceleration techniques, including RI-J and COSX, which dramatically improve the computational cost of these calculations at a very small cost in error, and these were used here. Experimentation with integral threshold settings indicated that the best trade-off between robust convergence and computational cost was to set the integral threshold (`thresh` in ORCA) to 1e-12 and the primitive batch threshold (`tcut` in ORCA) to 1e-13; these values were subsequently adopted by the ORCA package to be defaults in future versions of ORCA. ORCA's *tight* convergence settings were employed. Extensive benchmarking with various combinations of grid settings (both the exchange-correlation grid and the COSX grid) indicated that typical grids led to small numerical inconsistencies between energy and forces. In other words, there were discrepancies between the derivative of the energy with respect to coordinates and the computed forces due to grid incompleteness, and these errors were significant on the scale of errors with state-of-the-art MLIPs. In order to achieve sufficiently tight consistency, ORCA's `DEFGRID3` offered the best trade-off of convergence and cost. This corresponds to a pruned grid with 590 angular points for exchange-correlation and 302 for the final COSX grid.

A.1 Calculation Quality Filters

We apply the same quality checks as were applied to the OPoly26 dataset. We enforce several quality checks on the resulting DFT calculations before considering them in the final dataset:

- Referenced energies shall be smaller in magnitude than ± 150 eV or with a referenced energy/atom of < 10 eV/atom. This removes highly unreasonable configurations;
- Max per atom force shall not exceed $50\text{eV}/\text{\AA}$. This also removes highly unreasonable configurations;
- $S^2 < 0.5$ for open-shell metal-containing systems, $S^2 < 1.1$ otherwise. We enforce tighter constraints on metal-systems to avoid incorrect SCF solutions but allow full spin-unpairing which may occur in organic reactivity;
- Enforce alpha, beta, and total electron consistency with the integrated densities. This indicates insufficient grid density;
- ORCA errors where the final COSX exchange deviates considerably. This indicate convergence errors;
- Non-negative HOMO-LUMO gaps.

A.2 Computed Properties

The properties computed for each point in OPoly26 are the following:

1. Total energy (in eV)
2. Forces (in $\text{eV}/\text{\AA}$)
3. charge
4. spin
5. Number of atoms
6. Number of electrons
7. Number of ECP electrons
8. Number of basis functions
9. Unrestricted vs. Restricted
10. Number of SCF steps
11. Energy computed by VV10
12. S^2 expectation value

13. Deviation of S^2 from ideal
14. Integrated density (should be very close to the total number of electrons)
15. HOMO energy (in eV), α and β for unrestricted
16. HOMO-LUMO gap (in eV), α and β for unrestricted
17. Maximum force magnitude for a given atom in a given direction (fmax)
18. Mulliken charges (and spins if unrestricted)
19. Loewdin charges (and spins if unrestricted)
20. NBO charges (and spins if unrestricted) if the total number of atom ≤ 70
21. Any ORCA warnings that are generated
22. ORCA .gbw files and densities will be made available in the near future

B Polymer Compositions

B.1 General Sanitization

All polymer repeat units are represented by a polymer SMILES string, such as `/*CC*/` for polyethylene. SMILES representations of polymer repeat units are sanitized by i) verifying that the SMILES is valid with the RDKit package,[55] and ii) enforcing that all polymer SMILES strings contain exactly two `*` characters, corresponding to the two points of connection between repeat units. To ensure that a representative number of repeat units are present in each simulation cell, we filter out any polymer repeat units that contain more than 50 total atoms. This choice ensures that, for example, the alternating copolymer with 150 atoms/chain have at least an A-B-A copolymer chain architecture.

B.2 Traditional Polymers

The majority of the traditional polymer SMILES strings are sourced from the RadonPy benchmark dataset of 1,077 unique homopolymers.[27] According to the RadonPy paper, these 1,077 polymers were selected from the PoLyInfo database,[28] which contains 15,335 homopolymers, based on having the largest number of recorded experimental property measurements. To provide a further diversity of polymer compositions, we also hand-collected 85 unique homopolymers from the Bicerano Polymer Handbook[29]. Filtering and sanitizing these SMILES strings yields our final dataset of 840 traditional polymer compositions. In Figure 4, we highlight the general polymer families present in the Traditional Polymer compositions.

B.3 Fluoropolymers

Due to the lack of open-source databases of experimentally synthesized fluoropolymer SMILES strings, we instead collect example fluoropolymer compositions from the OpenMacromolecularGenome (OMG).[32] OMG consists of approximately 12 million unique polymer compositions that have been generated by applying 17 known polymer template reactions (such as step growth or chain growth addition) to a curated list of 77,281 commercially available small molecule reactants. Although all of the polymer compositions in OMG are not guaranteed to be synthesizable, this polymer generation process helps to ensure that compositions in OMG can be attributed to a proposed synthetic pathway.

From this dataset of 12 million polymer compositions, we first filter the compositions to check for SMILES validity (see B.1) and identify any polymer composition with at least one F atom, resulting in approximately 2.5 million fluoropolymer compositions. Then, to ensure that we sample as diverse a range of fluoropolymers as possible, we separate each of the fluoropolymers into their 17 associated polymer reaction templates. Within each polymer reaction template, we sort the polymer compositions by their fluorine content (as a fraction of total number of atoms) and then uniformly sample from the lower, middle, and upper thirds of this distribution. Since the fraction of fluorine in a polymer strongly influences its electronic and physical properties, this sampling strategy serves to ensure that OPoly26 contains polymers with a diverse range of

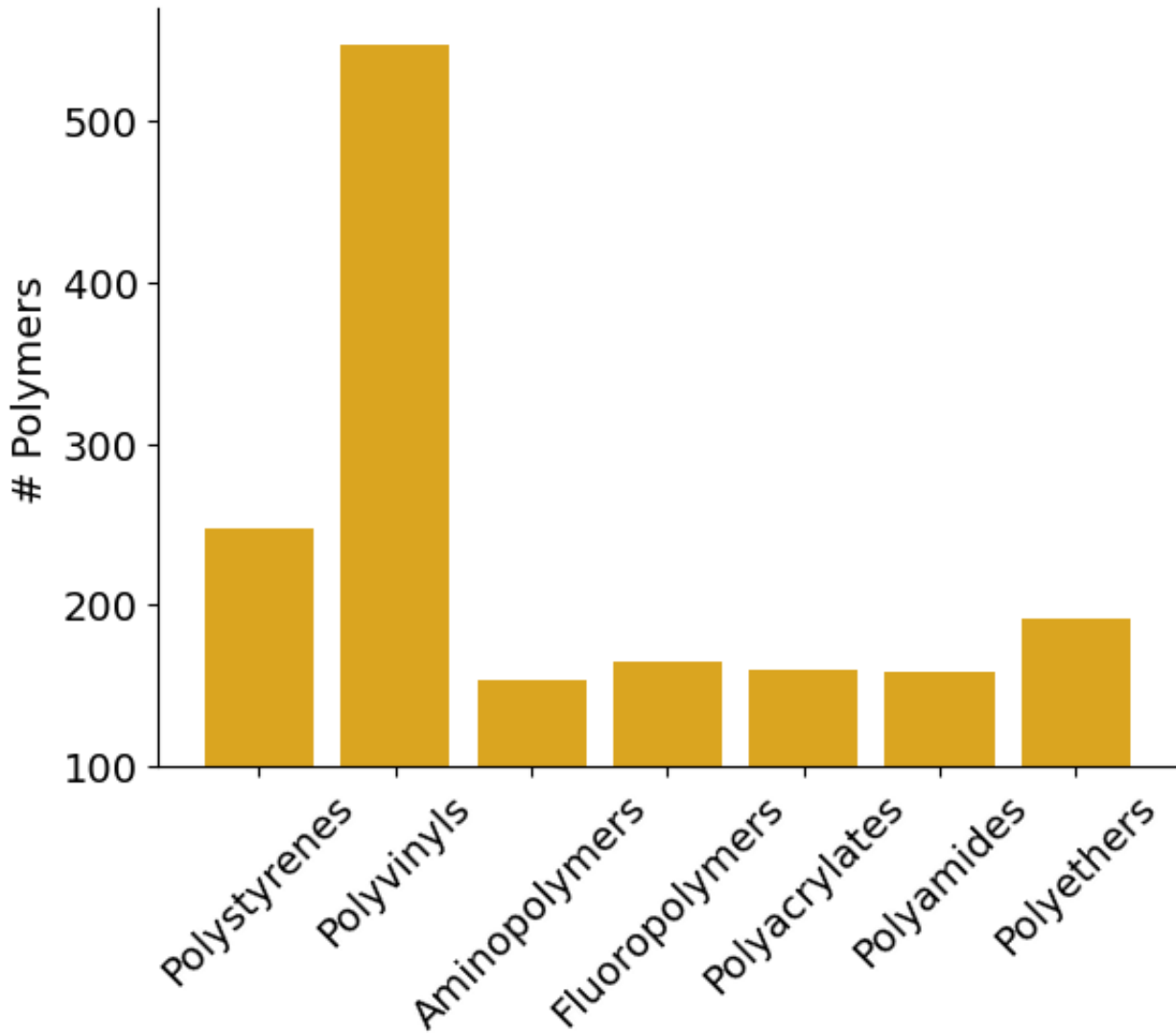


Figure 4 Overview of the polymer families present in the Traditional Polymer compositions. Polymer families are determined by defining a SMARTS substructure pattern for each polymer family and checking if each Traditional Polymer composition matches this pattern.

fluorine content. Similarly, uniformly sampling across all 17 polymer reaction templates ensures that we capture polymer compositions synthesized by various synthetic pathways. Altogether, we obtain 521 unique fluoropolymer compositions. We depict several illustrative fluoropolymer structures in Figure 5

B.4 Optical Polymers

We obtain optical polymer compositions from the chemical space of conjugated polymers provided by Aldeghi et al.[10], which was originally experimentally explored by Bai et al.[34]. Notably, this conjugated polymer library consists of prescribed copolymers that are comprised of 9 diboronic acid/acid ester (A) monomers and 706 dibromo (B) monomers, resulting in a total library of 6354 candidate copolymers. In this work, we respect these original A/B monomer assignments such that all copolymers are formed by the combination of one A monomer with one B monomer.

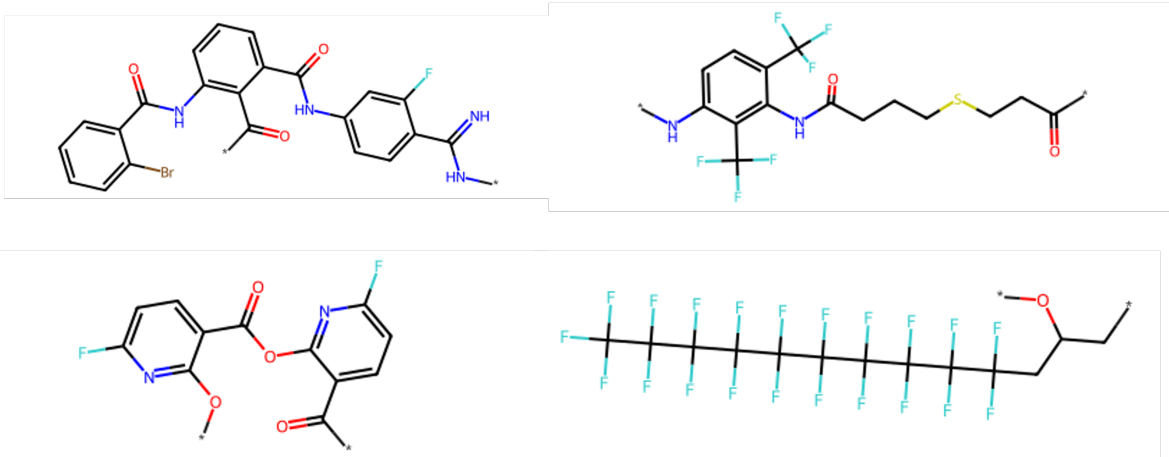


Figure 5 Illustrative examples of the fluoropolymer compositions present in OPoly26, depicting polymers with a wide range of fluorine content.

B.5 Polymer Electrolytes

All polymer electrolyte compositions are obtained from the PolyGen dataset of 6,024 unique polymers[37–39]. Notably, these polymer compositions are based off of hypothetical homopolymers that could be synthesized from a known condensation polymerization route. After sanitizing these compositions, we then represent all compositions with RDKit descriptors, (implemented through the *RDKitDescriptors* class of the DeepChem package)[56]. In order to sample the most diverse monomers from this dataset, we then perform k-means clustering on these featurized monomers (with $k=10$) and randomly sample 30 monomer compositions to give 300 unique polymer electrolyte compositions.

B.6 Ion-Inserted Polymers

Ion-inserted polymer systems were constructed as follows. Equilibrated polymer configurations in PDB format, obtained from prior classical molecular dynamics simulations, were used as the starting structures. For each polymer, a set of twenty ions was randomly selected from a curated library of forty common monoatomic and polyatomic ions (see listing in Table 6).

The selected ions were inserted into the equilibrated polymer matrices using the GROMACS molecular simulation package (version 2023.4). The `insert-molecules` utility was employed to place each ion template into the simulation box through stochastic trial placements, automatically rejecting overlapping configurations. This ensured physically realistic ion–polymer packing without manual adjustments. After insertion, all generated PDB files were standardized by correcting element symbols and assigning formal residue charges based on canonical oxidation states, with special handling for polyatomic species to preserve their stoichiometric and charge balance. For multi-atom ions, internal bonding information (CONECT records) was reconstructed from reference templates and appended to each combined polymer–ion structure while retaining the original polymer connectivity. The resulting outputs consisted of validated, charge-balanced PDB systems containing polymers with randomly distributed ions, complete connectivity information, and consistent metadata. These systems were then subjected to 2000 steps of MLIP-MD with UMA-s-1 OMol task, after which ion-containing subsystems were extracted for DFT simulations.

B.6.1 Lipids

To span a diverse set of common lipids in different bilayer environments, we extracted lipid simulation snapshots from the NMRLipid database [45]. We sampled simulations at 10 ns interval using all simulations listed in the NMRLipid database fitting with the following criteria: simulated with one of the following force fields (CHARMM, Slides, lipid14, lipid17, GROMOS, OPLS, Berger), longer than 20 ns, parsable with MDAnalysis [57], and contained atom charge information. The final set contained 47 different lipid types sampled from 674 simulations.

B.7 Polymer Architectures

As inputs, RadonPy takes in a SMILES string representation of the repeat unit sequence, the number of atoms in each polymer chain, the polymer type (including homopolymer, alt. copolymer, or random copolymer) and the number of polymer chains in the simulation cell. RadonPy then utilizes a self-avoiding random walk procedure to produce initial bulk amorphous cells. All chains are treated as atactic, and chain architectures are limited to linear homopolymers and copolymers, including alternating and random copolymers.

C MD Details

To generate large quantities of polymer structures, we carried out a series of classical all-atom MD simulations using the LAMMPS MD suite[46] and the RadonPy tools made available by Hayashi et al.[27] To facilitate the automation of MD calculations, RadonPy generates and runs LAMMPS input decks.

Classical MD calculations use fully periodic boundary conditions (PBCs). Standard Velocity Verlet time integration, with a timestep of 1 fs is used for MD production runs. This timestep is paired with the application of the SHAKE to all bonds with hydrogens (effectively fixing the lengths of these bonds). Where applicable, a Nosé-Hoover thermostat and barostat are applied with time constants of 100 and 1000 fs respectively.

System preparation procedures (detailed in the SI) leverage a “21-step” compression-decompression procedure proposed by Abbott et al.,[58] that uses alternating NPT (isothermal-isobaric) and high-temperature NVT (isothermal-isochoric) annealing phases to accelerate polymer dynamics (assuming time-temperature superposition). We opt to anneal the system at 600 K. This approach accelerates the equilibration of polymer melt configurations and defines a physically meaningful correlation time when sampling pseudo-independent simulation frames. As a final caveat, note that in a few cases 600 K may be insufficient to produce independent frames (e.g., polyimides); chain relaxation dynamics can be quite slow, and chain length dependent ($\tau \propto N^2$ up to $\tau \propto N^{3.4}$).

All classical MD uses a modified version of the General Amber FF (GAFF2),[59, 60] which is a generic atomistic potential, expressed in a convenient class 1 style. Specifically, GAFF2 includes harmonic bonds and angles, Fourier-style proper dihedrals, and cosine-style improper dihedrals. Van der Waals interactions are expressed in the standard 12-6 Lennard-Jones form with standard Lorentz-Berthelot mixing rules and incorporate switching functions to smoothly approach zero at 12 Å. Coulomb interactions were evaluated in real space up to an 12 Å cutoff and interactions beyond the cutoff were evaluated with the PPPM k-space solver using a relative error tolerance of 1e-6. Atomic electric charges were assigned using RadonPy[27] and were computed using the RESP method[61] and electrostatic potentials derived from DFT calculations performed at the ω B97M-D3BJ level on isolated, hydrogen-capped monomers.[50] Standard Amber intramolecular pairwise exclusion rules were applied in which 1-4 intramolecular interactions were scaled by 0.5 for LJ terms and 0.833 for Coulomb terms. Further force field parameterization details (including charge assignment, cutoffs, heteratom mixing, and intramolecular exclusion rules) are covered in the Supplemental Information (Section C.1), and the original RadonPy[27] manuscript.

C.1 MD Force Field

All calculations use a modified version of the General Amber FF, GAFF2, which is a generic atomistic potential.[59, 60]. As highlighted above, intramolecular potential energies are expressed in a convenient class 1 style; all bonds and angles are treated harmonically. The Fourier-style proper dihedrals (with angle ϕ) can be expressed via,

$$E = \sum_{i=1}^m K_i [1 + \cos(n\phi - d_i)] \quad (1)$$

while improper dihedrals are expressed via the cosine form, i.e.,

$$E = K [1 + d \cos(n\phi)]. \quad (2)$$

VDW interactions consistently follow a standard 12-6 Lennard-Jones form. However, there is a short period of initial relaxation dynamics (during which coulombic interactions are switched off) that applies a simple radial cutoff of 3 angstroms to the 12-6 LJ potential. All subsequent runs apply a Charmm-style switching function to the LJ potential that ramps the energy smoothly to zero between 8 and 12 angstroms (rather than having a discrete radial cutoff distance). The proposed benefit of this switching function is to reduce artifacts associated with the discontinuous change in the intermolecular potential at a discrete radial cutoff. Finally, we note that heteroatom mixing is arithmetic for LJ diameters, and geometric for the interaction strength parameter.

Intramolecular exclusion rules from Amber are adopted, meaning the LJ and coulombic interactions exclude atoms on the same molecule separated by 1 or 2 bonds (known as 1-2 and 1-3 interactions). Following the amber FF defaults, 1-4 interactions are scaled down by a factor of 0.5 for LJ, and 5/6 for coulombic interactions.

Coulombic interactions are handled differently; real-space interactions use a fixed cutoff of 12 angstroms (i.e., no switching functions are applied), whereas long-range electrostatics are handled via the P³M algorithm, which involves mapping atomic charges onto a fine mesh or grid. P³M settings are configured to target a per-atom force tolerance (quantified by the RMS error divided by a reference force, representing the pairwise interaction of two monovalent ions) of 10⁻⁶ (dimensionless). All other long-range solver settings are the LAMMPS suite defaults. Atomic partial charges are set as described in more detail below, as well as in the RadonPy paper.^[27] To ensure pair interactions aren't missed, neighbor lists are updated on each step in which an atom moves more than half the skin distance (set to 2Å).

C.2 System Preparation

System preparation follows the details provided in the RadonPy paper; in short this is a multistage system preparation procedure, where:

1. RDKit's conformer generator (ETKDG version 2) generates the initial molecular topology of a family of H-terminated repeat units from a SMILES string, which are
2. geometry optimized / energy minimized via a Molecular Mechanics calculation with the General Amber FF and generic charges.
3. The 4 most energetically stable conformers are then selected and DFT-optimized, and
4. fixed atomic charges are calculated using the RESP charge scheme, ensuring charge neutrality.
5. Individual chains are then polymerized from these repeat units via a self-avoiding random walk algorithm.

Options are provided to generate homopolymers, random, alternating, or block copolymers as random walks. Options are exposed in the RadonPy suite to specify fractions of co-monomers. Tacticity (atactic, isotactic, syndiotactic) is available as a secondary option. All polymer chains considered in our calculations are treated as atactic. All polymer chains are capped with a hydrogen termination group.

C.2.1 Preparation of Bulk (Amorphous) Polymer Cells

We opt to prepare two sets of cells – primarily, we focus on preparing boxes with 10 (approx.) 500-atom chains. In practice, this means that the degree of polymerization of our polymers (and in many cases, really oligomers) is variable, to keep the number of atoms per chain fixed. We note that these cells are approximately half the size of the 10000 atom cells prepared in the RadonPy manuscript. Having said that, we do prepare very small supplemental oligomer cells with just 3 100 atom chains; these cells are prepared only because it is impractical to run high-throughput DFTB MD calculations (described in a later section) on larger cells.

Subsequently, there is an initial packing procedure (described fully in Ref. 27) involving:

6. Creating an initial low density (0.05 g/cm³) structure by translating and rotating N chains, placing each chain into the box such that there are no overlaps.
7. Geometry optimization is then used to relax the initial configuration, followed by

8. 20 ps of 300 K NVT dynamics, with a reduced timestep (0.1 fs), and
9. 1 ns of dynamics with a NH thermostat, while temperature is ramped from 300 K to 700 K.
10. Finally, 1 ns of 700 K dynamics is carried out with a NH thermostat, while the cell is deformed until a density of 0.8 g/cm³ is achieved.

Steps (7-9) neglect coulombic interactions, but retain LJ interactions, with a fixed radial cutoff of 3 angstroms (in contrast, to the production runs detailed above). For more granular detail, refer to the RadonPy manuscript,[27] where each of these steps is described in full. Subsequently, we use a modified version of the equilibration schedule proposed by Larsen and co-workers. This procedure is sometimes referred to as a “21 step” procedure, which makes the procedure sound unnecessarily complicated. In short, it boils down to a multi-stage annealing procedure, consisting of a compression and decompression phase, with 3 discrete steps up (0.1, 3, 5), and 4 steps down (2.5, 0.5, 0.05 GPa, 1 atm) in pressure.

After each incremental step up (or down) in pressure,

1. 300 K NPT dynamics are run with a barostat enforcing the higher (or lower) pressure.
2. Next, there is an annealing step, with high-temperature NVT dynamics (at 600 K or 1000 K, depending on the speed of the chain’s dynamics).
3. The system is re-thermalized via 300 K NVT dynamics; a NH thermostat cools the system down and enforces the target temperature, prior to continuing with the compression-decompression cycle.

The principle of step 2 is to accelerate chain relaxation, based on a time-temperature superposition type assumption. On this basis, we choose to increase the length of the high-temperature NVT dynamics stages during the decompression phase; specifically, we use 50 ps of 600 K (or 1000 K) of NVT dynamics during the compression phase, whereas 500 ps runs are used during decompression. The final 300 K, 1 atm target state was also lengthened, using 1 ns of high-temperature annealing, a 10 ps re-thermalization run (NVT at 300 K), and then 800 ps of 300 K, 1 atm NPT dynamics. For a full equilibration schedule, see below.

Table 4 Equilibration schedule detailing each of the 21 steps in the compression-decompression cycle used to prepare bulk amorphous polymer cells.

Cycle #	Ensemble	T, P	Time [ps]
1	NVT	$T_{\max} = 600$ K (or 1000 K)	50
		300 K	50
	NPT	300 K, .1 GPa	50
2	NVT	600 K (or 1000 K)	50
		300 K	100
	NPT	300 K, 3 GPa	50
3	NVT	600 K (or 1000 K)	50
		300 K	100
	NPT	300 K, $P_{\max} = 5$ GPa	50
4	NVT	600 K (or 1000 K)	500
		300 K	100
	NPT	300 K, 2.5 GPa	5
5	NVT	600 K (or 1000 K)	500
		300 K	10
	NPT	300 K, 0.5 GPa	5
6	NVT	600 K (or 1000 K)	500
		300 K	10
	NPT	300 K, 0.05 GPa	5
7	NVT	600 K (or 1000 K)	1000
		300 K	10
	NPT	300 K, 0 GPa (1 atm)	800

C.2.2 Preparation of Solvated (Infinite Dilution) Polymer Cells

Due to practical time constraints, we opt to prepare a series of infinite dilution solvated cells; specifically consisting of a single 500 atom chain, and 4500 solvent atoms (although the established pipeline can prepare multi-chain solvated cells with some limitations). A full list of solvents and polymers is provided in the appendix. As with our bulk cells, the GAFF2 force field is used to represent both polymer and solvent at atomistic resolution. The sole exception to this is water, which we use with a 3-site flexible water model (TIP3P/FW) that was modified for use with long-range (Ewald style) electrostatics.[62] Exact parameters for the water model are provided in Section C.3. Initial preparation stages are identical to those outlined previously. As with the bulk cells, RESP charges are derived from DFT-level calculations of the polymer's constituent repeat units and solvent molecules respectively. After using RadonPy to polymerize a single chain (homopolymer, alternating copolymers, or random copolymer) via a self-avoiding random walk, we stamp one of a handful of chosen solvent molecules into a periodic box using Packmol.[63] Packmol tries to neatly pack the solvent molecules around the lone polymer chain (representing a chain at infinite dilution) such that it achieves the desired target density of 1 g/cm³ we selected. Since Packmol is entirely ignorant of any force field parameters or information, we use a

1. preliminary energy minimization of the Packmol cell to clean up the initial configurations. To ensure the configuration is well-behaved, we subsequently
2. do an initial NVT relaxation at a lower temperature (100 K). A reduced timestep (0.1 and then 0.5 fs) is used with intermittent velocity reselects from a Maxwell-Boltzmann distribution.
3. Nose-Hoover style temperature and pressure control is used to gradually ramp the temperature up from 100 K to the target of 300 K at 1 atm.
4. NVT relaxation at 300 K with a few velocity reselects, followed by
5. NPT relaxation at 300 K and 1 atm.
6. 200 ps of high-temperature NVT dynamics are used (at 600 K).
7. Ramp down temperature to 300 K, followed by NVT thermalization at 300 K.
8. A final period of NPT equilibration at 300 K and 1 atm (200 ps)

C.3 Solvents

Table 5 Solvents used in MD polymer simulations. The density values represent the inputs densities used to construct the initial MD simulation cells. Water was simulated with the TIP3P(Ewald) force field[62]. All other solvents were simulated with the GAFF2 force field[59] with modified fluorocarbon parameters[60]. Out-of-distribution (OOD) solvents were not included in either the train set of OPoly26 nor OMol25.

Solvent Name	SMILES	Density (g/cm ³)	FF Parameters	Train/OOD
Water	O	1.00	TIP3P[62]	Train
Acetone	CC(=O)C	0.791	GAFF2[59, 60]	Train
Acetonitrile	CC#N	0.786	GAFF2[59, 60]	Train
Benzene	C1=CC=CC=C1	0.876	GAFF2[59, 60]	Train
Cyclohexane	C1CCCCC1	0.779	GAFF2[59, 60]	Train
Hexane	CCCCCC	0.661	GAFF2[59, 60]	Train
Octane	CCCCCC	0.703	GAFF2[59, 60]	Train
Propanol	CCCO	0.803	GAFF2[59, 60]	Train
1,2,4- Trichlorobenzene	C1=CC(=C(C=C1Cl)Cl)Cl	1.46	GAFF2[59, 60]	Train
Dimethyl Formamide	CN(C)C=O	0.95	GAFF2[59, 60]	Train
Tetrahydrofuran	C1CCOC1	0.888	GAFF2[59, 60]	Train
Chloroform	C(Cl)(Cl)Cl	1.49	GAFF2[59, 60]	Train
Phenol	C1=CC=C(C=C1)O	1.07	GAFF2[59, 60]	Train
Dichloromethane	C(Cl)Cl	1.33	GAFF2[59, 60]	Train
Toluene	CC1=CC=CC=C1	0.867	GAFF2[59, 60]	Train
Methanol	CO	0.792	GAFF2[59, 60]	Train
n-Heptane	CCCCCC	0.684	GAFF2[59, 60]	Train
1,4-Dioxane	O1CCOCC1	1.033	GAFF2[59, 60]	OOD
Formic Acid	O=CO	1.220	GAFF2[59, 60]	OOD
N-Methyl-2-Pyrrolidone	CN1CCCC1=O	1.028	GAFF2[59, 60]	OOD
Decalin	C1CCC2CCCC2C1	0.896	GAFF2[59, 60]	OOD
Tetrachloroethylene	ClC(Cl)=C(Cl)Cl	1.622	GAFF2[59, 60]	OOD

C.4 Ion insertion MLIP-MD

Table 6 Ions used in MLIP-MD simulations. Test ions were not included in the train set of OPoly26, but may be present in OMol25.

Ion Name	Chemical Formula	Train/Test
Aluminum Ion	Al^{3+}	Train
Tetrafluoroborate	BF_4^-	Train
Bromide	Br^-	Train
Calcium Ion	Ca^{2+}	Train
Triflate	$CF_3SO_3^-$	Train
Acetate	CH_3COO^-	Train
Perchlorate	ClO_4^-	Train
Chloride	Cl^-	Train
Cyanide	CN^-	Train
Cobalt Ion	Co^{2+}	Train
Carbonate	CO_3^{2-}	Train
Cesium Ion	Cs^+	Train
Copper Ion	Cu^{2+}	Train
Iron Ion	Fe^{2+}	Train
Fluoride	F^-	Train
Bicarbonate	HCO_3^-	Train
Iodide	I^-	Train
Potassium Ion	K^+	Train
Lanthanum Ion	La^{3+}	Train
Lithium Ion	Li^+	Train
Magnesium Ion	Mg^{2+}	Train
Sodium Ion	Na^+	Train
Ammonium	NH_4^+	Train
Nickel Ion	Ni^{2+}	Train
Nitrate	NO_3^-	Train
Hexafluorophosphate	PF_6^-	Train
Phosphate	PO_4^{3-}	Train
Sulphate	SO_4^{2-}	Train
Strontium Ion	Sr^{2+}	Train
Zinc Ion	Zn^{2+}	Train
Hydronium	H_3O^+	Test
Hypochlorite	ClO^-	Test
Sulfite	SO_3^{2-}	Test
Thiocyanate	SCN^-	Test

The equilibrated ion-inserted polymer systems were used as the initial configurations for machine-learning molecular dynamics (ML-MD) simulations. All simulations were performed using the Atomic Simulation Environment (ASE) framework interfaced with the FAIRChem machine-learned interatomic potential (MLIP) package.[64] Atomic interactions were modeled using the UMA-S-1P1 neural network potential, which was selected for its balanced accuracy across organic and inorganic chemistries relevant to ion-polymer interactions.[19] Each polymer-ion configuration was converted into an ASE Atoms object and simulated under periodic boundary conditions applied in all three directions. The total formal charge of each system was automatically parsed from the PDB metadata and passed to the ML potential to maintain charge consistency. MD simulations were carried out in the canonical ensemble (NVT) at 300 K using a Berendsen thermostat with a relaxation time constant of 100 fs. The equations of motion were integrated with a 1 fs time step, and atomic velocities were initialized from a Maxwell–Boltzmann distribution at the target temperature. All production trajectories were run for 2 picoseconds before extracting clusters for single point DFT calculations.

C.5 DFTB

We enriched the configuration space sampled for the set of Traditional Homopolymers through semiempirical quantum MD applied to simulate both reactive and nonreactive conditions. To this end, we simulate polymers with the third-order Density Functional Tight Binding (DFTB) method,[65] the DFTB+ code,[66] and the 3ob-3-1 parameter set (available at <http://www.dftb.org>),[67] which is a general parameter set for organic molecules. The electronic structure was evaluated at the gamma point without spin polarization and with Fermi-Dirac thermal smearing with the electronic temperature set equal to the ionic thermostat temperature.[68] DFTB-MD simulations were performed with NVT dynamics at 300 K and 600 K using 3D periodic equilibrium amorphous configurations (<300 atoms) prepared with classical MD through RadonPy. Simulations were run for at least 20,000 time steps, with a 0.2 fs time step. A small set of highly reactive simulations probing radiation-induced chemistry of silicones were performed following the protocols in Ref. [52].

D Reactivity

Diversity in reactive configurations, with minimal bias toward specific chemical motifs, is ensured by selecting a single bond for dissociation randomly from a candidate pool curated to mitigate C–H bond overrepresentation and exclude nonphysical pathways involving aromatic atoms. By avoiding prespecified product structures, the AFIR search remains unbiased toward known reaction outcomes, allowing the discovery of reaction pathways over the course of data generation. We apply this protocol to homopolymer and copolymer systems, as well as bulk and solvated chains. To introduce additional electronic diversity, 10% of chains are protonated and 10% deprotonated near the reactive bond, and 10% undergo single-electron oxidation and 10% single-electron reduction (AFIR generation of these radical systems had a high failure rate, so a comparatively small sample of final data points in the dataset were derived from these reduced or oxidized reactions). These procedures generate rich training data with local environments where charge and unpaired electrons can modulate reactivity in these polymer system.

To more faithfully capture the polymer chain environment, each AFIR trajectory is initialized from a unique chain conformation where an atom at each chain end is fixed in space. We impose these constraints because polymer chains, being macromolecular in nature, have limited access to other conformations due to the entropic constraint of being confined by sizable molecular fragments that make up an overall chain. After AFIR trajectories are generated, frames are subsampled by the same procedure put forward in OMol25[24] and trimmed to under 250 atoms as preparation for DFT calculations. With this procedure (detailed further in Appendix D), we obtain high chemical diversity across tens of thousands of single-bond dissociation events and incorporate approximations that capture the differences in chemistry between polymers and small molecules.

D.1 AFIR Preparation

Polymer chain structures from MD trajectories are encoded using a modified `Molecule` class in Architector[69], which contains additional attributes for repeat unit representations, solvent molecules, and chain end atoms. RDKit[55], ASE, and OpenBabel facilitate the reconstruction of molecular connectivity and geometry from MD-generated structures, correcting periodic artifacts and broken bonds by comparing covalent radii with wrapped interatomic distances. When the indices of chain end atoms (i.e., those that share a bond with the hydrogen cap on the terminal repeat unit) are not explicitly specified in the MD structure file, chain termini are located with RDKit substructure matching. Metadata such as repeat unit(s) and solvent type are parsed from MD frame filenames and mapped to the curated SMILES library for that category (e.g., traditional, optical, fluoropolymer, electrolyte, solvent).

D.1.1 Bond Selection

Bonds are first scored and ranked based on local chemical environment metrics. A final bond is then selected at random from a filtered, high-scoring subset of bonds, allowing stochastic diversity in bond selection while baking in chemical intuition.

Polymers are predominantly hydrocarbon macromolecules. To address this inherent skew in bond-type

distribution in the interest of exploring a diverse set of bond dissociation reactions in polymer systems, we enforce that only 10% of the subset of high-scoring bonds contain hydrogen. Additionally, we limit ring-containing bonds to be at most 10% of the subset, in order to prevent an over-selection of such bonds when scoring is based on local atomic density. In no case, however, are aromatic bonds present in the subset. Dissociation reactions that involve aromatic bonds are likely to lead to convergence failures under standard DFT protocols, and are not frequently studied reactions due to their incredibly low probability of occurrence. Bond dissociation reactions that result in forming triplet oxygen are also similarly avoided.

For bulk versus solvated chain systems, we employ differently tailored bond scoring procedures:

Bulk reactivity: In bulk systems, we are interested in reactivity at the point of highest density to stay faithful to the condensed-phase environment of bulk polymer. Candidate bonds are therefore required to be (a) at least 5.0 Å away from all chain ends (as defined in Section D.1) and (b) within 5.0 Å of the polymer system's center of mass. If no such bond satisfies these criteria, which can be the case for high rigidity chains, the center of mass cutoff is increased to 10.0 Å. Scores based on local atomic density are then assigned to the filtered subset of bonds, promoting the selection of densely packed, interior bonds to approximate bulk-like reactivity.

Solution reactivity: In different solvation environments, a polymer chain's conformations vary significantly. For example, polymer chains in poor solvent prefer self-interaction as opposed to interaction with the solvent molecules, leading to the polymer chains adopting a tight, globular conformation with chain ends tucked into the center. Atomic density-based scoring metrics are ill-suited for such cases because here, we are interested in the chemical diversity of interfacial reactivity as opposed to bulk-like reactivity. For solvated systems we therefore penalize polymer bonds according to their proximity to chain ends, which encourages sampling from solvent-exposed regions. By ranking bonds based on their maximum distance from the closest chain end, we enrich the dataset with reactions at the polymer-solvent interface, especially for poorly solvated chains.

D.1.2 Pre-Trimming

Bulk and solvated chain systems containing more than 800 atoms require a pre-processing step of trimming before the reactive protocol can be applied, in order to minimize the cost of generating AFIR trajectories. At each trimming step, we assure that the reactive bond is re-indexed appropriately. Different trimming protocols are applied to polymers in bulk and solution:

Bulk systems: Bulk chain systems are trimmed down to be at most 500 atoms. At random, a radial cutoff between 4.0 and 6.0 Å is selected to determine the size of spherical, "protected zones" created around each atom in the selected bond for dissociation. Atoms in these zones are off-limits for trimming, so that we can preserve the chemical environment surrounding the dissociation event during data generation. Starting from the chain end furthest from the reactive bond, we iteratively remove one repeat unit at a time, capping the newly exposed atom in the next repeat unit with hydrogen, until either the target atom count is reached or further truncation would encroach upon the protected zones. Substructure matching with RDKit is employed to remove atoms in a given repeat unit at each step. This procedure repeats until the target atom count is achieved, iterating through the chain ends in order of farthest to the reactive bond to closest. If the system iterates through all chain ends and still has the targeted number of atoms, the protected zone cutoff radius is decreased by 1.0 Å, and the process is repeated.

Solvated systems: When more than 150 chain atoms are present, solvated chain systems are trimmed down to at least 800 atoms. This maximum atom threshold is higher than for bulk, so that the reactivity at the polymer-solvent interface may be explored with an adequate number of solvent molecules present. If necessary, solvent molecules are translated to fully wrap the polymer chain in cases where periodic boundaries cause fragmentation. The same trimming algorithm described for bulk systems is then applied, with an additional step where solvent molecules within or overlapping with the protected zones are iteratively kept until atom count thresholds are met.

D.1.3 Charge Diversification

To maximize chemical diversity, one third of all structures undergo hydrogenation while another third undergoes dehydrogenation to introduce net charge in the system before the AFIR calculation. SMILES

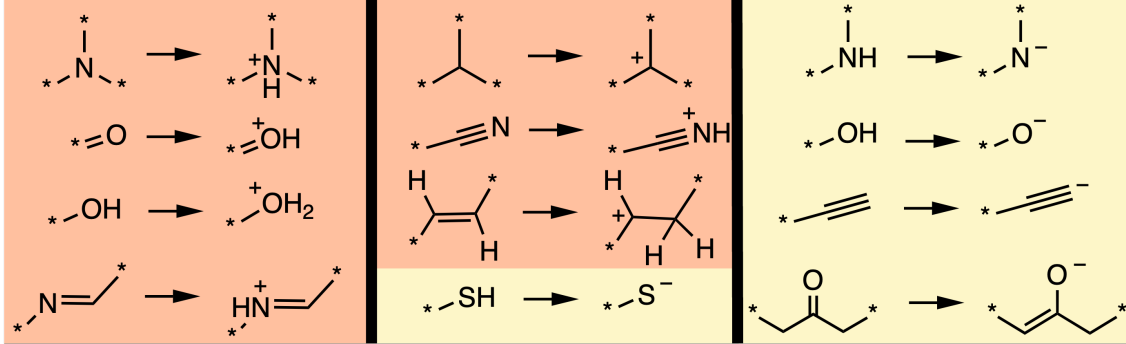


Figure 6 Functional group transformations employed to incorporate net positive (in orange) or negative (in light yellow) charge in a polymer chain prior to AFIR trajectory generation.

arbitrary target specifications (SMARTS) are employed for RDKit substructure matching to identify a subset of functional groups, illustrated in Figure 6, present in the system that can undergo these transformations. For each polymer system, all substructure matches corresponding to the available functional groups for a given transformation (hydrogenation or dehydrogenation) are first enumerated. Only substructure matches that overlap with the reactive region surrounding the bond selected for dissociation (i.e., within 5 Å of the bond atoms) are eligible for selection. A functional group match from the eligible list is then randomly selected to undergo transformation. The following distinct steps are taken for a given transformation:

Hydrogenation: The position of the new hydrogen atom (H) is computed based on the position and connectivity of the heavy atom to which it will be bonded. A geometric heuristic is applied to place the hydrogen with a bond length of 1.01 Å in a direction according to the heavy atom’s number of neighbors (N):

- $N = 3$, H is placed along the normal to the plane defined by the three neighbor atoms, oriented away from the nearest neighbor to avoid poor placement.
- $N = 2$, H is positioned opposite the bisector of the two neighboring bond vectors.
- $N = 1$, H is placed opposite to the existing bonded neighbor.

If the generated position of the new hydrogen atom does not fall within 0.5 Å of other atoms, the transformation is applied to the system. If there is overlap, hydrogenation is attempted four more times. After successful hydrogenation, the net charge of the polymer is adjusted accordingly.

Dehydrogenation: Carbocations are generated through dehydrogenation in this work, whereas all other dehydrogenation pathways correspond to deprotonation events. Because hydrocarbons are over-represented in the dataset, the selection probabilities for dehydrogenation are reweighted. Specifically, when the carbocation-forming SMARTS is present among eligible substructure matches, its selection probability is set to $\frac{1}{14}$. The complementary probability $\frac{13}{14}$ is distributed uniformly among the remaining SMARTS patterns. After a SMARTS is selected according to these modified probabilities, a hydrogen atom within the corresponding substructure match is removed. Bond re-indexing is performed to preserve the identity of the bond selected for dissociation, and the net charge of the polymer system is appropriately modified.

D.2 AFIR Protocol

After the above preparation steps, we apply the AFIR method used in OMol25[24] with a few modifications. We adapt the method to run single-ended searches, in which only the reactant structure and atom indices of the bond breaking are specified. Chain end atoms are fixed in space using ASE constraints. The bond breaking cutoff is increased to $5 \times$ the equilibrium bond length to allow for minimally-guided yet greater exploration along the potential energy surface. A maximum force of 10 eV/Å and a force step of 0.75 eV/Å are used to more efficiently drive reactivity along the polymer chain, compensating for the greater structural inertia of macromolecular-like systems compared to small molecules. The Universal Model for Atoms (UMA)[19] trained on the OMol25 dataset is employed to provide energies and forces for AFIR calculations, under the turbo inference setting. AFIR generated frames are then filtered to retain unique structures that capture the

reaction pathway, using the algorithm described in OMol25. For solvated chains, the first relaxation with applied force is excluded from structure filtering.

D.3 Post-Trimming

To prepare AFIR-generated structures for DFT calculations, each geometry is trimmed to contain less than 250 atoms. The last filtered AFIR structure is used to determine which atoms will be removed from all other structures along the AFIR trajectory, assuming this structure underwent the largest changes in bonding connectivity. Building onto the method used in pre-trimming, protected zones with a radius between 4.0 and 6.0 Å are generated around atoms in the reactive bond as well as all atoms that demonstrate altered connectivity from the starting geometry. As in pre-trimming, atoms are removed one repeat unit at a time—starting with the chain ends farthest from the reactive site—followed by hydrogen-capping of newly exposed chain ends. Trimming proceeds until either the protected zone is reached or the atom count threshold is satisfied. If the resulting structure still exceeds 250 atoms, the protected zone cutoff is iteratively reduced by 1.0 Å, and the trimming is repeated. The same set of atoms deleted from the last AFIR structure is then removed from all other filtered structures, with appropriate hydrogen capping applied at chain ends where repeat units were extracted.

E Extracting Substructures from Trajectories

E.1 Polymers

From each MD trajectory, we sample 8 frames from the simulated annealing portion and 4 frames from the equilibration portion, resulting in preferential sampling of non-equilibrium polymer structures. Within each of these portions of the MD trajectory, we calculate the root mean square displacement (RMSD) between all polymer structures and sample the frames of the trajectory with the largest dissimilarity to all other structures in the trajectory. In the ML MD and DFTB simulations, frames are randomly sampled from across the trajectory. After sampling a frame from a trajectory, a polymer residue is selected at random and either a spherical shell or a "cylindrical" shell (including several neighboring residues and their close contacts) is selected up to a randomly chosen maximum number of atoms (150, 200, or 300). These shells include entire monomers and therefore terminate at the connection point between monomer repeat units. This shell is extracted and capped with hydrogen atoms. We ensure that the extracted substructure is appropriately contracted across periodic boundaries to a compact form suitable for molecular DFT

E.2 Lipids

For lipid systems, we cycled through head, linker, and tail moieties of randomly selected lipid molecules in an MD simulation, attempting to extract clusters of them and their environment. Each moiety's environment was defined as all other heads, linkers, or tails with any atom within 3 Å of the center moiety but excluding any atoms more than 10, 5, or 4 Å from the center moiety (opting for the largest such cluster within the maximum atom limit of 300 atoms). Cut bonds were capped with H's except for phosphate groups which were capped with -OMe groups. For each MD simulation, 30 structures were obtained by this procedure.